

High-frequency magnetization dynamics of individual atomic-scale magnets

S. Krause,^{*} A. Sonntag,[†] J. Hermenau, J. Friedlein, and R. Wiesendanger

Department of Physics, University of Hamburg, Jungiusstraße 11, 20355 Hamburg, Germany

(Received 14 September 2015; revised manuscript received 11 January 2016; published 4 February 2016)

The magnetization dynamics of individual nanomagnets is studied by spin-polarized scanning tunneling microscopy, combining real-time telegraphic noise analysis with pump-probe schemes. A transition between two Arrhenius regimes is observed as a function of temperature. The switching rates at high temperature are found to be orders of magnitude lower than expected from the extrapolation from the low-temperature regime. A four-state hopping model of magnetization reversal is developed to interpret the experimental results in terms of nucleation, annihilation, and propagation.

DOI: [10.1103/PhysRevB.93.064407](https://doi.org/10.1103/PhysRevB.93.064407)

Nucleation, annihilation, and domain wall propagation are the most fundamental microscopic processes of magnetization reversal [1,2]. Understanding and controlling the mechanisms that favor or hinder magnetization reversal is crucial for the development of high-speed spintronic applications for data storage, information transmission, and sensing.

In previous spin-polarized scanning tunneling microscopy (SP-STM) studies it was shown that the thermally activated magnetization reversal of Fe/W(110) nanomagnets consisting of less than 100 atoms is realized by nucleation and propagation instead of a coherent rotation of all magnetic moments of the nanomagnet [3–5]. Here, the domain wall behaves like a quasiparticle moving along the [001] direction. Although the monodomain state is not present during the magnetization reversal, the temperature-dependent switching rate can be described by an Arrhenius law. The experiments in Refs. [3–5] were all based on real-time recording of the telegraphic noise of the spin-polarized tunnel current I . A typical telegraphic noise measurement is shown in Fig. 1(a). As I depends on the relative orientation between tip and sample magnetization [6,7], switching between antiparallel (state **0**) or parallel (state **1**) orientation between the sample and fixed tip magnetization generates a two-state signal. This is reflected in a modulation of the tip-to-sample distance z in the constant current mode of SP-STM. The temporal resolution of this method is ultimately limited by the bandwidth of the transimpedance amplifier (TIA), being typically in the kHz regime. Consequently, only the lifetime *between* two switching events is readily accessible, whereas the dynamics of the microscopic processes *during* magnetization reversal is hidden.

Pump-probe schemes allow the observation of processes that are much faster than the temporal resolution of the TIA. In combination with STM, a temporal resolution down to the low ps or even fs regime has successfully been realized with electrical or optical pumping [8,9]. In the pioneering work of Loth *et al.*, SP-STM experiments have been combined with an all-electronic pump-probe scheme, thereby achieving a temporal resolution in the low ns regime, while maintaining magnetic and atomic resolution [10]. Within the present study we use SP-STM to investigate the magnetic ground state dynamics of a single nanomagnet with uniaxial magnetic

anisotropy over a wide temperature and switching-rate regime. The experimental data are interpreted in terms of an analytical hopping model, thereby providing insight into the microscopic processes during magnetization reversal. Switching is hindered at low temperature by a high annihilation rate after nucleation, whereas the switching rate is comparable to the nucleation rate at high temperature.

I. EXPERIMENTAL SETUP

Our experiments were performed under ultrahigh vacuum conditions with a pressure below 1×10^{-8} Pa using a home-built SP-STM setup at variable temperatures with coaxial cabling for the sample bias voltage line (bandwidth ≈ 100 MHz). Within our experimental setup, the entire microscope including the tip is cooled to maximize the thermal stability. In the direct vicinity of the sample, a GaAs/GaAlAs diode is mounted, serving as a temperature sensor. A continuous flow He cryostat with a proportional—integral—derivative (PID) controlled resistive heater at the cooling finger allows for a precise adjustment of the system temperature T to any set-point between 27 K and 300 K. Bulk Cr tips [11] as well as Fe coated W tips [7] served as magnetic probes. The W(110) substrate was prepared by annealing in oxygen atmosphere and subsequent high-temperature flashes [12]. Depositing Fe onto this substrate leads to the pseudomorphic formation of atomic-scale monolayer nanoislands that are found to be ferromagnetic at cryogenic temperatures [4]. They exhibit an in-plane uniaxial magnetic anisotropy with the easy axis of magnetization lying in the $[1\bar{1}0]$ direction [13,14]. Due to thermal activation, the nanomagnets frequently switch their magnetization between the two ground states **0** and **1**, being in the mean state $\frac{1}{2}$ when integrating over time.

II. REAL-TIME OBSERVATIONS DURING PUMP-PROBE EXPERIMENTS

In the work of Loth *et al.*, the spin relaxation times of Fe-Cu dimers were probed [10]. A magnetic field was used to align the spin of the dimer, and pumping into the excited state was achieved by a voltage pulse via inelastic scattering of tunneling electrons. The relaxation into the ground state was probed by a second voltage pulse which was applied with varying delay time Δt after the pump pulse. In contrast to the scheme of Loth *et al.*, we measure the transition rate

^{*}skrause@physnet.uni-hamburg.de

[†]asonntag@physnet.uni-hamburg.de

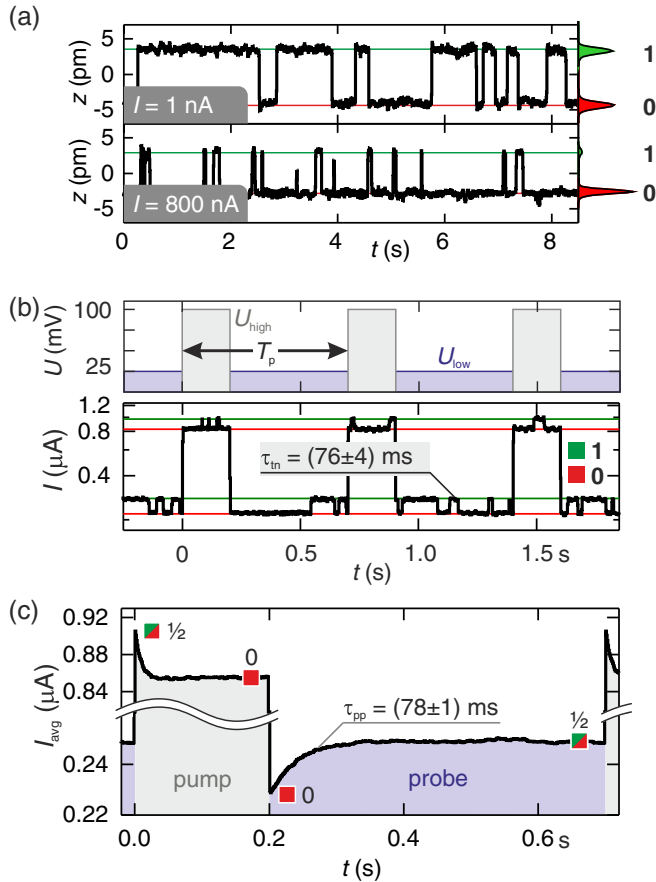


FIG. 1. (a) Telegraphic noise $z(t)$ on a nanomagnet at low and high I at closed feedback loop, and respective data histograms. ($U = 100 \text{ mV}$, $T = 45 \text{ K}$) (b) Top: Periodic sequence of high and low tunnel bias. Bottom: Resulting noise I on a thermally switching nanomagnet at constant tip-sample distance. (c) Averaged noise signal during one cycle, calculated from $I(t)$ in (b).

between the two energetically degenerate ground states of an individual nanomagnet, implying that no magnetic field is applied. Moreover, a high tunnel current of spin-polarized electrons is used for pumping.

The basic idea of this spin-transfer torque based pump-probe scheme is illustrated in the following. In Fig. 1(a), the tip-to-sample distance variation $z(t)$ is shown for an individual nanomagnet at closed feedback loop for $I = 1 \text{ nA}$ and $I = 800 \text{ nA}$, respectively. At low I , the nanomagnet is in thermal equilibrium, being in a mean state $\frac{1}{2}$, as can be seen from the upper graph of Fig. 1(a). When I is on the order of a few hundred nA, as shown in the lower graph of Fig. 1(a), the spin-transfer torque generated by a high spin-polarized tunnel current forces the magnetization of the nanomagnet into one of the two states [3,5,15].

In order to record the telegraphic noise during and after the injection of a high spin-polarized tunnel current, a periodic modulated bias voltage U (with period T_p) is applied between the nanomagnet and the magnetic SP-STM tip being held at constant distance. In Fig. 1(b), the results of such an experiment are exemplarily shown for $T_p = 0.7 \text{ s}$. Every cycle starts by setting the bias to $U_{\text{high}} = 100 \text{ mV}$ for 0.2 s.

This generates a short high spin-polarized tunnel current of $I = 850 \text{ nA}$. The pulse is followed by a period of low bias $U_{\text{low}} = 25 \text{ mV}$ for 0.5 s, resulting in a reduced spin-polarized tunnel current of $I = 250 \text{ nA}$. Within the low-current and high-current sequences, a two-level modulation of the spin-polarized tunnel current is observed on a much smaller scale, reflecting the switching behavior of the nanomagnet. Analyzing the telegraphic noise at low I , the intrinsic mean lifetime τ_{in} between two consecutive switching events can directly be determined [4], resulting in $\tau_{\text{in}} = (76 \pm 4) \text{ ms}$ for the given nanomagnet.

In Fig. 1(c), $I(t)$ has been averaged to $I_{\text{avg}}(t)$ over numerous cycles. Here, telegraphic noise is no longer visible. However, an exponential decay is found in $I_{\text{avg}}(t)$ whenever U is changed. This behavior reflects the alignment and thermal relaxation of the sample magnetization when changing from the low to the high I regime and vice versa in each cycle. At $t = 0$, the nanomagnet is in thermal equilibrium (state $\frac{1}{2}$). During the pulse of high I it is driven into the magnetic state **0**, as indicated by the significant decrease of I_{avg} during the pulse. When the pulse ends (at $t = 0.2 \text{ s}$), the nanomagnet thermally relaxes back into the state $\frac{1}{2}$, as can be seen from the temporal evolution of I_{avg} . Consequently, the nanomagnet is pumped into one preferred state during the high I pulse, and its relaxation back into its thermal equilibrium state is probed after the pulse at low I . Note that the decay time during pumping is much smaller than for probing, reflecting the higher switching rate of the nanomagnet at high I due to significant Joule heating. As can be shown from solving the rate equations within a model of a simple two-state system reversing its magnetization by surmounting one single activation energy barrier, the characteristic magnetic decay time λ after pumping is given by the intrinsic mean lifetime τ of the nanomagnet: $\lambda = \tau/2$. From the data in Fig. 1(c) a mean lifetime from the pump-probe experiment $\tau_{\text{pp}} = (78 \pm 1) \text{ ms}$ is found for the relaxation into thermal equilibrium.

Both values, τ_{in} and τ_{pp} , are in perfect agreement with each other. Consequently, the intrinsic mean lifetime τ can be determined either by real-time telegraph noise experiments (τ_{in}) or by applying pump-probe schemes (τ_{pp}). In the latter, no real-time observation is necessary, making this method suitable for systems exhibiting magnetic ground state dynamics that cannot be resolved by telegraphic noise experiments.

III. PUMP-PROBE EXPERIMENTS ON FAST SWITCHING NANOMAGNETS

In our pump-probe experiments on nanomagnets with switching rates that exceed the bandwidth of our TIA, we apply a pump-probe scheme that is schematically depicted in Fig. 2(a). Within each pump-probe cycle, a pump pulse forces the nanomagnet out of thermal equilibrium (state $\frac{1}{2}$) into one preferred magnetic state, e.g., state **0**. After pumping, the nanomagnet stochastically relaxes back into state $\frac{1}{2}$. A probe pulse is applied after varying Δt to map the evolution of the magnetic state.

The experimental realization of this pump-probe scheme with SP-STM is depicted in Fig. 2(b). Initially, the tip-to-sample distance is adjusted at closed feedback loop. Here, the tunnel current set-point equals the desired pump pulse

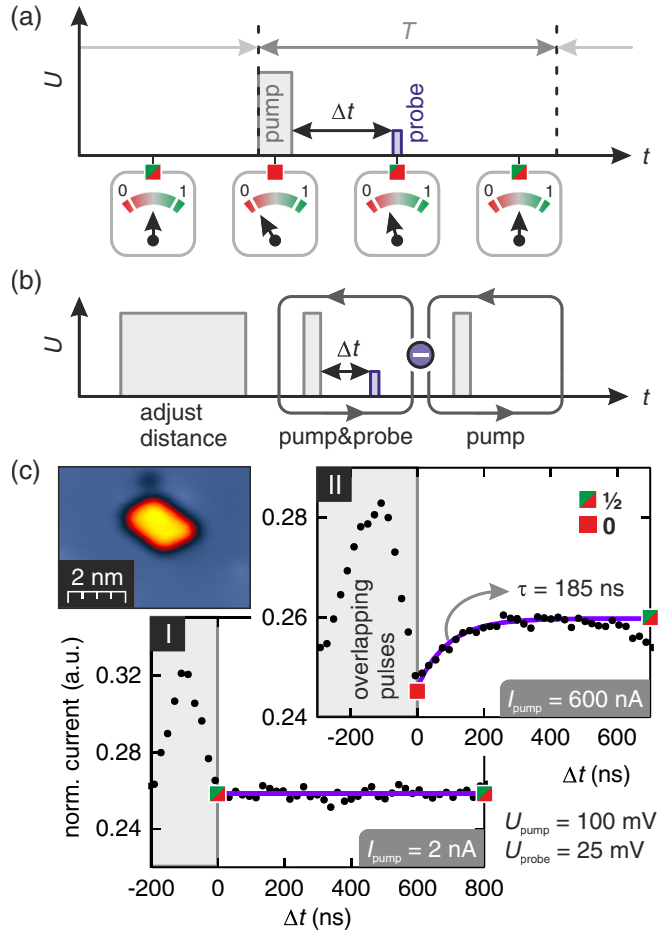


FIG. 2. (a) Basic idea of the spin-transfer torque-driven pump-probe scheme. (b) Experimental realization of the pump-probe scheme with SP-STM (see text for details). (c) Pump-probe experiment on a nanomagnet (inset: topography). (I) Low pumping current I_{pump} : No relaxation is observed. (II) High I_{pump} : A relaxation into thermal equilibrium is observed. Fitting the data yields the mean lifetime τ . ($T = 42$ K).

amplitude I_{pump} . Once the distance is adjusted, the feedback loop is switched off and U is set to zero. Consecutively, a pump pulse is generated, followed by a probe pulse of low I at a given delay time Δt . This pump-probe cycle is repeatedly applied to the tunnel junction. The short spin-polarized tunnel current pulses are not resolved individually due to the limited bandwidth of the TIA, and the average during the cycle is measured. To isolate the contribution of the probe pulse and to increase the signal-to-noise ratio, a differential measurement is realized. The sequence of pump-probe cycles is followed by a sequence of pump-only cycles in which the probe pulse is left out. The averaged spin-polarized tunnel current is now lower compared to the full pump-probe cycle due to the missing contribution of the probe pulse. Therefore, I is modulated by ΔI at the chopping frequency f_{mod} . Since ΔI is the average spin-polarized tunnel current during the probe pulse, it gives a measure of the alignment between tip and sample magnetization averaged over the (fixed) probe pulse length. The pulse pattern is generated by a two-channel pulse generator (Agilent 81130A or 88150A). The first channel is

used to generate the pump pulses, while the second generates the probe pulses that are chopped with f_{mod} . Both channels are added using a signal adder, and the pulse pattern is fed to the sample via a remote-controlled RF switch. The resulting modulation of I is measured by a lock-in amplifier.

To map the evolution of the magnetic state after pumping, the experiment is repeated for different Δt . From $\Delta I(\Delta t)$, the characteristic magnetic decay time λ can be extracted by fitting an exponential.

An exemplary pump-probe measurement on a nanomagnet is shown in Fig. 2(c). Pump and probe spin-polarized tunnel current pulses were injected into the nanomagnet, and the variation in I was recorded as a function of Δt . The results for $\Delta I(\Delta t)$ show a characteristic triangular-shape feature when pump and probe pulses overlap, resulting from the nonlinearity in the $I(U)$ curve of the tunnel junction [8,10]. For $\Delta t > 0$, the pulses do not overlap, and ΔI is given by the average current during the probe pulse. In Fig. 2(c) I, the spin-polarized pump pulse amplitude is set to $I_{\text{pump}} = 2$ nA. A flat line is observed for $\Delta t > 0$, indicating the nanomagnet being in the mean state $\frac{1}{2}$ throughout the experiment. Hence, the nanomagnet has not been affected by the pump pulse and remains in thermal equilibrium. In Fig. 2(c) II, I_{pump} was increased by a factor of 300 with respect to the situation in I. Now an exponential decay is observed after the pump pulse. The combined action of spin-transfer torque and Joule heating during the pump pulse forces the nanomagnet into the state 0 , and it decays back into thermal equilibrium (mean state $\frac{1}{2}$) for $\Delta t > 0$. Fitting the data with an exponential reveals $\tau = 185$ ns. In this experiment I during the probe pulse is sufficiently high that pumping into state 0 cannot be neglected, resulting in the decrease of ΔI for $\Delta t > 600$ ns. In this regime, the excitation is probed by the pump pulse that is applied shortly following the probe pulse.

IV. QUANTITATIVE VALIDATION OF THE EXPERIMENTS

A direct comparison between pump-probe experiments and real-time telegraphic noise observation for the validation of the experimental findings is not possible as the latter technique can only be used for lifetimes larger than a few milliseconds. The identification of individual switching events of shorter lifetimes is mainly hindered by mechanical noise in the kHz regime (e.g., the resonance frequencies of the scanner) overlaying the telegraphic signal. However, the mean lifetime τ between two consecutive switching events of a random telegraph signal can be determined in frequency space. To obtain the lifetime using spectral analysis, we measure the power spectral density $S(f)$ of I using a HP 89410A spectral analyzer. For a symmetric random telegraph signal, $S(f)$ is given by [16]

$$S(f) \propto \frac{1}{1 + \left(\frac{f}{f_c}\right)^2}. \quad (1)$$

Consequently, $S(f)$ is constant for frequencies f much smaller than the characteristic frequency f_c and decays with f^{-2} for $f \gg f_c$. The characteristic frequency is related to τ by

$$f_c = \frac{1}{\pi\tau}. \quad (2)$$

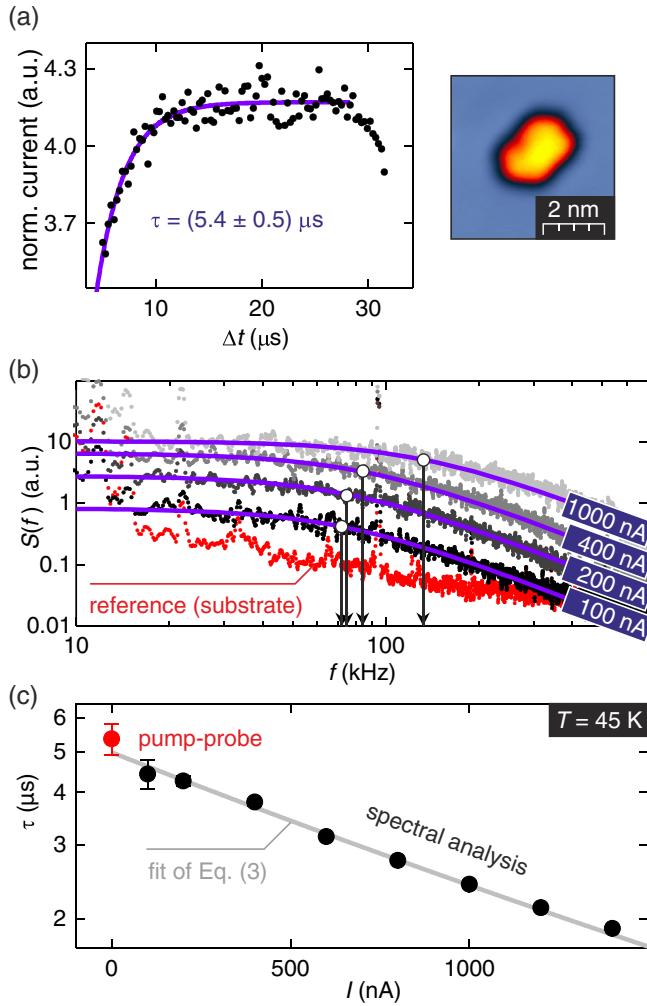


FIG. 3. (a) Pump-probe measurement on the island shown in the inset, $T = 45$ K. (b) Power spectral density measured as a function of tunnel current ($U = 100$ mV). (c) Comparison between results obtained using the pump-probe method and the power spectral measurement. A fit is used to extrapolate the spectral analysis to $I = 0$.

To compare the two methods we choose a superparamagnetic nanoisland that is expected to have a lifetime of a few μs at the measurement temperature of $T = 45$ K, so that both the spectral analysis and the pump-probe method are applicable. Figure 3(a) shows a pump-probe experiment performed on the nanomagnet. Its topography is shown in the inset. From the data, an exponential decay of the normalized tunnel current is observed as a function of Δt . Fitting yields a mean lifetime of $\tau_{\text{pp}} = (5.4 \pm 0.5) \mu\text{s}$.

To measure such a short lifetime with the spectral measurement, a bandwidth of the TIA on the order of 500 kHz is needed. In the present setup, this bandwidth can be achieved when the gain of the TIA is reduced to 10^4 V/A. However, due to the small gain, the tunnel current has to be increased to a few hundred nA to achieve a reasonable signal-to-noise ratio. Consequently, current-induced effects are expected not to be negligible. Current-dependent spectral measurements are shown in Fig. 3(b). Compared to the reference spectrum that was taken with the tip positioned above the substrate

($I = 200$ nA), a significantly higher $S(f)$ is obtained when the tip is positioned above the nanomagnet. The increase on the island is caused by its thermal magnetization switching, as can be concluded from the characteristic $S(f)$ shape [cf. Eq. (1)]. Below 15 kHz considerable noise is found, which is attributed to mechanical vibrations inside the STM. The strong peak at 90 kHz is caused by electrical noise, probably from a power supply.

Fitting the experimental data with Eq. (1), the characteristic frequency $f_c(I)$ is obtained. The fits and corresponding $f_c(I)$ are indicated in Fig. 3(b). The mean lifetime $\tau(I)$ was calculated from $f_c(I)$ according to Eq. (2). They are shown in Fig. 3(c). Obviously, τ decreases with increasing tunnel current. Joule heating is not negligible for the tunnel currents used in this experiment, which thus significantly shortens the mean lifetime. Additionally, the switching behavior of the nanomagnet at high I is expected to be asymmetric due to the spin-transfer torque of the tunneling electrons. However, this effect only slightly affects the mean lifetime $\tau(I)$. Using a Néel-Brown model, the lifetimes were fitted, taking into account Joule heating that is linear in I [5] and omitting the influence of the spin transfer torque:

$$\tau(I) = \nu_0^{-1} \exp\left(\frac{E_b}{k_B(T + c_T I)}\right), \quad (3)$$

with E_b being the effective activation energy barrier, ν_0 is the effective attempt frequency, k_B is the Boltzmann factor, and c_T is a constant that reflects the effective differential heating of the nanomagnet (in K/nA). The fit is used to extrapolate to $I = 0$, yielding an intrinsic mean lifetime of $(5.0 \pm 0.2) \mu\text{s}$. Within the error bars, this is in very good agreement with the finding of the pump-probe method.

The Arrhenius behavior of the lifetimes as function of temperature and the perfect agreement between the two experimental methods show that the pump-probe scheme yields reliable results that are quantitatively comparable to results obtained with conventional methods. Consequently, combining pump-probe SP-STM experiments and real-time observation enables the determination of lifetimes ranging from hours to nanoseconds, and thereby allows us to study the lifetime of an individual nanomagnet over a wide temperature range.

V. EXPERIMENTAL RESULTS

Such experiments were performed for three different nanomagnets shown in Fig. 4(a). For each nanomagnet τ has been determined via real-time telegraphic noise observations in the low switching rate regime ($\tau > 10^{-2}$ s) and pump-probe experiments for high switching rates ($\tau < 10^{-4}$ s). For $10^{-4} < \tau < 10^{-2}$ s the determination of τ is hindered due to the low signal-to-noise ratio of the system in this frequency band. In Fig. 4(b), the respective T -dependent switching rates $\nu = \tau^{-1}$ are shown in an Arrhenius plot for all three nanomagnets. As can be seen from the data, each of the nanomagnets shows a characteristic switching behavior, with the data points lying on two crossing straight lines. In the Arrhenius plot, the slope of the lines corresponds to the effective activation energy barrier E_b for magnetization reversal. From the data it is obvious that E_b of every nanomagnet is constant within the low and the

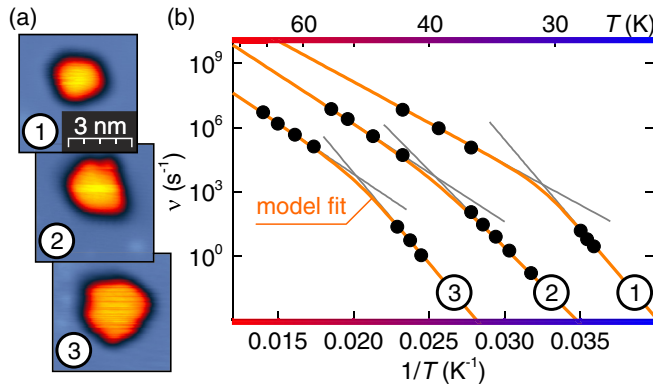


FIG. 4. (a) The nanomagnets under investigation. (b) T -dependent switching rates of each nanomagnet. A crossover between two Arrhenius regimes is observed. Orange: four-state hopping model fit.

high T ranges, and undergoes a transition within a T window of about 10 K. Moreover, ν at high T is generally found to be orders of magnitude lower than expected from extrapolating the Arrhenius behavior at low T .

It is known that material parameters like magnetic exchange and anisotropy can change with T . A smooth deviation from the Arrhenius behavior can be expected in this case, but not a sharp transition within a window of a few Kelvin, as observed in our experiments. A sudden change of magnetic exchange or anisotropy with drastic consequences for the magnetic properties with increasing T is unlikely. Moreover, no significant variations in the magnetic properties of a closed monolayer film of Fe/W(110) have been observed in a much broader T window [13], so we exclude T -dependent material parameters to be the origin of the experimental findings. In a theoretical investigation using Monte Carlo calculations, a transition from a one-droplet to a multidroplet nucleation was observed with increasing T , resulting in two distinct Arrhenius regimes [17]. In the situation of multidroplet nucleation, a second domain wall is created before the first domain wall is annihilated. Both domain walls can interact with each other, thereby changing the Arrhenius switching behavior. In our experiments, the characteristic time scale of the transition between the two Arrhenius regimes is on the order of milliseconds. Consequently, one domain wall has to be trapped inside the island for about a millisecond before it can interact with the second domain wall. In our opinion this is unlikely, since the microscopic processes are known to happen on a much faster timescale of pico- or even femtoseconds [18]. Within the original model for the coherent rotation of all magnetic moments, a \sqrt{T} temperature dependence of the attempt frequency is predicted [19,20]. This T dependence is omitted in most studies, as it usually changes insignificantly compared to the exponential term. When the T dependence is taken into account, the lifetimes at higher temperature are increased compared to the case where the temperature dependence is neglected, which is in qualitative agreement with our experimental findings. We included the temperature dependence and fitted the model to our data. It turned out that the fit with or without the temperature dependence gives

almost the same results. Consequently, even when taking into account the temperature dependent attempt frequency, the model of a single activation energy barrier cannot be used to describe our observations. In summary, none of these theoretical approaches correctly describes our experimental findings.

VI. FOUR-STATE HOPPING MODEL

Based on simple arguments, we develop an analytical four-state hopping model that accounts for all the microscopic processes that are involved in the magnetization reversal: nucleation, annihilation, and propagation. Its scheme is depicted in Fig. 5(a). In the model, the nanomagnet can be found at any time in one of four magnetic states $\mathbf{0}$, $\mathbf{01}$, $\mathbf{10}$, and $\mathbf{1}$ with probabilities P_0 , P_1 , P_{01} , and P_{10} , respectively. Here, $\mathbf{0}$ and $\mathbf{1}$ are the two monodomain ground states. $\mathbf{01}$ and $\mathbf{10}$ are metastable states where the magnetization within a nucleus volume is reversed with respect to the rest of the nanomagnet. Nucleation, annihilation and propagation is modeled by hopping between the states at intrinsic rates ν_n , ν_a , and ν_p , respectively. They follow Arrhenius laws:

$$\nu_i = \nu_{0,i} \exp\left(-\frac{E_i}{k_B T}\right), \quad i = n, a, p. \quad (4)$$

Here, $\nu_{0,n}$, $\nu_{0,p}$, $\nu_{0,a}$, E_n , E_p , and E_a are the effective attempt frequencies and activation energy barriers. The potential landscape for the magnetization reversal within our hopping model is shown in Fig. 5(b). It is known that the magnetocrystalline anisotropy can be drastically higher at the rim of a nanomagnet due to the reduced coordination of the rim atoms [21]. This hinders the formation as well as the annihilation of a nucleus. Hence, in our model the effective activation energy barriers E_n for nucleation and E_a for annihilation are introduced.

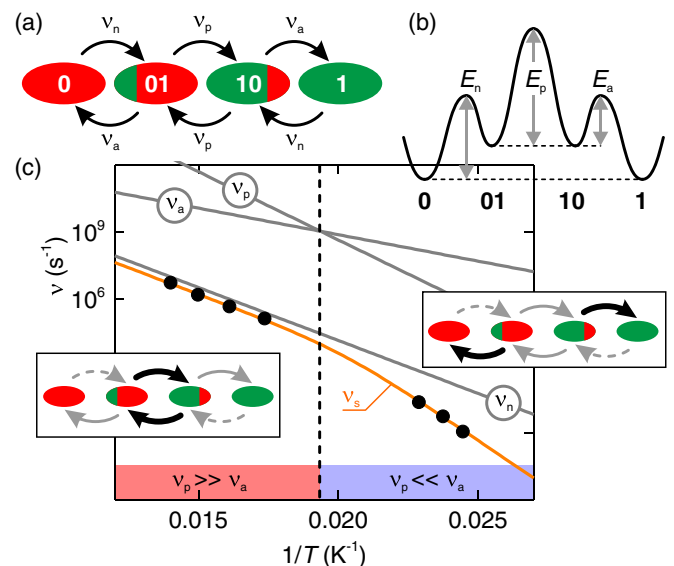


FIG. 5. (a) Schematics and (b) energy landscape of the four-state hopping model. (c) Experimental data for nanomagnet “3”, fitted by the hopping model (orange), and respective rates ν_n , ν_a and ν_p . Insets: Dominating hopping paths (thick arrows) at low and high T , respectively.

The domain wall propagation inside the nanomagnet is a very complex process. We implement an effective activation barrier E_p and attempt frequency $\nu_{0,p}$ in our model to mimic the microscopic details of the domain wall propagation between nucleation and annihilation. Magnetization reversal is triggered by nucleation, implying that $\nu_n \ll \nu_a$ and $\nu_n \ll \nu_p$. We calculate the effective switching rate ν_s between the two ground states **0** and **1** by solving the rate equations, yielding

$$\nu_s = \left(2 + \frac{\nu_a}{\nu_p}\right)^{-1} \nu_n. \quad (5)$$

Hence, ν_s is given by ν_n reduced by a factor that depends on the ratio ν_a/ν_p . We find the asymptotic limits for low and high T :

$$\text{low } T: \nu_s^{\text{low}} = \nu_0^{\text{low}} \exp\left(-\frac{E^{\text{low}}}{k_B T}\right), \quad (6)$$

$$\text{high } T: \nu_s^{\text{high}} = \frac{1}{2} \nu_n. \quad (7)$$

Here, $E^{\text{low}} = E_n - E_a + E_p = E_{\text{act}}$ is the overall activation energy barrier for magnetization reversal, and $\nu_0^{\text{low}} = \frac{\nu_{0,n}\nu_{0,p}}{\nu_{0,a}}$ is the effective attempt frequency at low T . A distinct Arrhenius behavior is found for each T regime, in perfect agreement with our experimental results. The experiments in Ref. [4] have been performed in the low- T regime and therefore address the magnetization reversal over an effective activation barrier given by E_{act} . Note that the parameters E_p , E_a , $\nu_{0,p}$, and $\nu_{0,a}$ cannot explicitly be determined from the experiments in the low- T regime, because the effective switching rate results from the complex interplay between nucleation, annihilation and propagation. In our model, ν_s^{high} directly reflects the nucleation rate of the nanomagnet, implying that the effective attempt frequency and activation energy barrier for nucleation can directly be determined experimentally from the Arrhenius behavior in the high- T regime.

VII. FITTING THE EXPERIMENTAL DATA

Using the model, the experimentally obtained $\nu(T)$ for each nanomagnet are fitted. The resulting fit parameters are summarized in Table I, and the model fit curves are added to Fig. 3(b). The data for the nanomagnets ② and ③ in the low- T regime are in perfect agreement with the results of Ref. [4] in terms of activation energy barrier and attempt frequency, whereas nanomagnet ① deviates. In the high- T regime, E_n and $\nu_{0,n}$ are determined from the model. For all three nanomagnets, the nucleation process can be described by an effective activation energy barrier between 75 and 95 meV, and the respective attempt frequency for nucleation varies between 10^{13} and 10^{16} s^{-1} .

TABLE I. Results of fitting the four-state hopping model to the experimentally obtained data for each nanomagnet.

	①	②	③
$E^{\text{low}} = E_{\text{act}}$ (meV)	165	142	168
$E^{\text{high}} = E_n$ (meV)	76	91	94
$\nu_0^{\text{low}} = \frac{\nu_{0,n}\nu_{0,p}}{\nu_{0,a}}$ (s^{-1})	2.4×10^{30}	7.7×10^{21}	6.7×10^{20}
$2\nu_0^{\text{high}} = \nu_{0,n}$ (s^{-1})	1.3×10^{16}	4.6×10^{15}	4.0×10^{13}

To illustrate the model interpretation of the experimental findings, the fit results for the nanomagnet ③ are shown in Fig. 5(c). For exemplification, the open parameters are set to $\nu_{0,a} = \nu_{0,n}$ and $E_a = E_n/2$. At high T , $\nu_p \gg \nu_a$, implying that a nucleation event is immediately followed by the propagation of a domain wall. Annihilation is hindered, so the domain wall undergoes numerous backscattering events. Because of this annihilation site uncertainty, $\nu_s = \nu_n/2$. At low T , $\nu_p \ll \nu_a$. Propagation is hindered, and the nucleus is very likely to annihilate at its nucleation site. Only in very rare events can the domain wall propagate through the nanomagnet, finally resulting in a magnetization reversal. Consequently, $\nu_s \ll \nu_n$, but again follows an Arrhenius law, as can be seen from Fig. 5(c).

VIII. SUMMARY

In summary, we investigated the magnetization dynamics of individual nanomagnets over a wide temperature and switching rate range using SP-STM telegraphic noise experiments and applying pump-probe schemes. The finite and distinct effective activation energy barriers and attempt frequencies for the microscopic processes involved in the magnetization reversal are found to have drastic consequences for the T -dependent switching behavior of atomic-scale magnets. Our study reveals that the switching behavior does not follow one single Arrhenius law. Instead, a transition between two Arrhenius regimes is observed with increasing T , and the switching rate at high T is found to be orders of magnitude smaller than expected from an extrapolation from the low- T regime. An analytical four-state hopping model is developed to interpret the experimental results, indicating that ν at high T reflects the nucleation rate, whereas ν at low T results from the complex interplay between nucleation, annihilation, and propagation which drastically reduces the effective switching rate of the nanomagnets compared to the nucleation rate.

ACKNOWLEDGMENT

Financial support via Grants No. SFB 668-B4 and No. GrK 1286 from the Deutsche Forschungsgemeinschaft is gratefully acknowledged.

S.K. and A.S. contributed equally to this work.

- [1] W. Wernsdorfer, B. Doudin, D. Mailly, K. Hasselbach, A. Benoit, J. Meier, J.-P. Ansermet, and B. Barbara, *Phys. Rev. Lett.* **77**, 1873 (1996).
 [2] S. S. P. Parkin, M. Hayashi, and L. Thomas, *Science* **320**, 190 (2008).

- [3] S. Krause, L. Berbil-Bautista, G. Herzog, M. Bode, and R. Wiesendanger, *Science* **317**, 1537 (2007).
 [4] S. Krause, G. Herzog, T. Stapelfeldt, L. Berbil-Bautista, M. Bode, E. Y. Vedmedenko, and R. Wiesendanger, *Phys. Rev. Lett.* **103**, 127202 (2009).

- [5] S. Krause, G. Herzog, A. Schlenhoff, A. Sonntag, and R. Wiesendanger, *Phys. Rev. Lett.* **107**, 186601 (2011).
- [6] R. Wiesendanger, H. J. Güntherodt, G. Güntherodt, R. J. Gambino, and R. Ruf, *Phys. Rev. Lett.* **65**, 247 (1990).
- [7] R. Wiesendanger, *Rev. Mod. Phys.* **81**, 1495 (2009).
- [8] G. Nunes and M. R. Freeman, *Science* **262**, 1029 (1993).
- [9] O. Takeuchi, M. Aoyama, R. Oshima, Y. Okada, H. Oigawa, N. Sano, H. Shigekawa, R. Morita, and M. Yamashita, *Appl. Phys. Lett.* **85**, 3268 (2004).
- [10] S. Loth, M. Etzkorn, C. P. Lutz, D. M. Eigler, and A. J. Heinrich, *Science* **329**, 1628 (2010).
- [11] A. Schlenhoff, S. Krause, G. Herzog, and R. Wiesendanger, *Appl. Phys. Lett.* **97**, 083104 (2010).
- [12] M. Bode, S. Krause, L. Berbil-Bautista, S. Heinze, and R. Wiesendanger, *Surf. Sci.* **601**, 3308 (2007).
- [13] U. Gradmann, G. Liu, H. J. Elmers, and M. Przybylski, *Hyperfine Interact.* **57**, 1845 (1990).
- [14] H. J. Elmers, J. Hauschild, H. Höche, U. Gradmann, H. Bethge, D. Heuer, and U. Köhler, *Phys. Rev. Lett.* **73**, 898 (1994).
- [15] G. Herzog, S. Krause, and R. Wiesendanger, *Appl. Phys. Lett.* **96**, 102505 (2010).
- [16] M. J. Kirton and M. J. Uren, *Adv. Phys.* **38**, 367 (1989).
- [17] U. Nowak and D. Hinzke, *J. Appl. Phys.* **85**, 4337 (1999).
- [18] H. Stoll, M. Noske, M. Weigand, K. Richter, B. Krüger, R. M. Reeve, M. Hänze, C. F. Adolf, F.-U. Stein, and G. Meier, *Front. Phys.* **3**, 26 (2015).
- [19] M. L. Néel, *Ann. Géophys.* **5**, 99 (1949).
- [20] W. F. Brown, *Phys. Rev.* **130**, 1677 (1963).
- [21] P. Gambardella, A. Dallmeyer, K. Maiti, M. C. Malagoli, W. Eberhardt, K. Kern, and C. Carbone, *Nature (London)* **416**, 301 (2002).